


Polymorphonuclear MDSCs are enriched in the stroma and expanded in metastases of prostate cancer

Jiling Wen^{1,2†}, Gang Huang^{1,2†}, Sheng Liu³, Jun Wan^{3,4,5}, Xuechun Wang^{2,6}, Yini Zhu⁷, William Kaliney⁸, Chao Zhang⁶, Liang Cheng⁹, Xiaofei Wen^{1*} and Xin Lu^{2,7,8,10*} 

¹Department of Urology, Shanghai East Hospital, Tongji University School of Medicine, Shanghai, PR China

²Department of Biological Sciences, Boler–Parseghian Center for Rare and Neglected Diseases, University of Notre Dame, Notre Dame, IN, USA

³Department of Medical and Molecular Genetics, Indiana University School of Medicine, Indianapolis, IN, USA

⁴Center for Computational Biology and Bioinformatics, Indiana University School of Medicine, Indianapolis, IN, USA

⁵School of Informatics and Computing, Indiana University – Purdue University at Indianapolis, Indianapolis, IN, USA

⁶Translational Medical Center for Stem Cell Therapy and Institute for Regenerative Medicine, Shanghai East Hospital, Shanghai Key Laboratory of Signaling and Disease Research, School of Life Sciences and Technology, Tongji University, Shanghai, PR China

⁷Integrated Biomedical Sciences PhD Program, University of Notre Dame, Notre Dame, IN, USA

⁸Harper Cancer Research Institute, University of Notre Dame, Notre Dame, IN, USA

⁹Department of Pathology and Laboratory Medicine, Indiana University School of Medicine, Indianapolis, IN, USA

¹⁰Tumor Microenvironment and Metastasis Program, Indiana University Melvin and Bren Simon Cancer Center, Indianapolis, IN, USA

*Correspondence: Xin Lu, Department of Biological Sciences, Boler–Parseghian Center for Rare and Neglected Diseases, University of Notre Dame, Notre Dame, IN 46556, USA. E-mail: xlu@nd.edu; Xiaofei Wen, Department of Urology, Shanghai East Hospital, Tongji University School of Medicine, Shanghai 200120, PR China. E-mail: wenxiaofei2000@hotmail.com

† Co-first authors.

Abstract

Myeloid-derived suppressor cells with polymorphonuclear morphology (PMN-MDSCs) contribute to the progression and immune evasion of prostate cancer. However, the spatial distribution of tumor-infiltrating PMN-MDSCs in primary and metastatic prostate cancer, especially in the context of comparison between the epithelial and stromal compartments of the tumor, has not been characterized. Here, we describe a multicolor immunofluorescence staining study of 90 primary tumors, 37 lymph node metastases (all with matched primary tumors) and 35 bone metastases using archived samples. CD11b⁺ CD15⁺ cells were identified as PMN-MDSCs and pan-cytokeratin⁺ cells were identified as prostate epithelial cells. We found that, in both primary tumor and metastases, PMN-MDSCs infiltrate much more readily in the stromal area compared with the epithelial area of the tumor regions. In comparison to the stromal area of primary tumors, the stromal area of either lymph node metastases or bone metastases was infiltrated with more PMN-MDSCs. In primary tumors, stromal PMN-MDSCs were associated with vascularization, segmented neutrophils, patient age and close juxtaposition to neoplastic epithelial cells. These results reveal the stroma rather than the epithelia of prostate cancer as the major hotbed for PMN-MDSCs and support the role of PMN-MDSCs in the metastatic progression of prostate cancer.

Keywords: polymorphonuclear MDSC; prostate cancer; lymph node metastasis; bone metastasis; epithelial and stromal areas; tumor microenvironment; multicolor immunofluorescence staining

Received 20 September 2019; Revised 30 January 2020; Accepted 8 February 2020

No conflicts of interest were declared.

Introduction

Myeloid-derived suppressor cells (MDSCs) are a heterogeneous population of immature myeloid cells with potent immunosuppressing activity [1,2]. MDSCs are classified as polymorphonuclear (PMN-MDSCs) or monocytic (M-MDSCs). Prostate cancer (PCa) is the second most common cancer among men worldwide

[3]. We and others have reported that PMN-MDSCs are the predominant MDSC subset in PCa patients [4–6]. However, these studies focused on the detection of either circulating PMN-MDSCs or the overall frequency of tumor-infiltrating PMN-MDSCs without the distinction of the spatial distribution of PMN-MDSCs. Furthermore, studies so far have not compared the density of infiltrating PMN-MDSCs between primary and

metastatic PCa. To address these unmet needs, we performed a retrospective study using formalin-fixed paraffin-embedded (FFPE) samples from 90 primary tumors, 37 lymph node metastases and 35 bone metastases. Using multicolor immunofluorescence (mIF) staining, our goal was to characterize the spatial distribution of PMN-MDSCs in the epithelial and stromal areas. To the best of our knowledge, this is the first study that examines the spatial distribution of PMN-MDSCs in both primary and metastatic PCa.

Materials and methods

Clinical samples

Clinical samples were FFPE slides from tissue banks at three institutions: 49 prostatectomy primary tumors from South Bend Medical Foundation (SBMF); 20 primary tumors with 17 matched lymph node metastases and 26 independent bone metastases from MD Anderson Cancer Center (MDACC); 21 primary tumors with 20 matched lymph node metastases and 9 independent bone metastases from Indiana University School of Medicine (IUSM). De-identified archival tissues were obtained with approved IRB protocols from SBFM (IRB#13-09-1226), MDACC (IRB#PA14-0420), and IUSM (IRB#1808872882). Patient characteristics for the primary tumor cases are listed in Table 1. The patient characteristics for bone metastasis cases were unavailable.

Multicolor immunofluorescence staining

For the CD11b/CD15/pan-cytokeratin (pan-CK)/DAPI multicolor immunofluorescence (mIF) panel, antigen-retrieved slides were incubated with anti-CD11b rabbit antibody (AB133357, Abcam, Cambridge, MA, USA) at 1:2000 and CK mouse antibody (MA5-13156, Invitrogen, Carlsbad, CA, USA) at 1:100 overnight at 4°C. After washing, slides were incubated with AF594-conjugated-anti-rabbit IgG and AF647-conjugated-anti-mouse IgG for 2-h in the dark. After washing, slides were incubated with AF488-conjugated anti-CD15 mouse antibody (301910, BioLegend, San Diego, CA, USA) at 1:40 and DAPI for 2 h in the dark. For the CD11b/CD15/CD33/DAPI mIF panel, anti-CD33 mouse antibody (303402, BioLegend) was used at 1:100 instead of pan-CK antibody. For the CD31/CD8a/pan-CK/DAPI mIF panel, slides were incubated with anti-CD31 rabbit antibody (AB28364, Abcam) at 1:100 and anti-CD8a mouse antibody (372902, BioLegend) at 1:100 overnight at 4°C. After washing, slides were incubated with AF594-conjugated-anti-rabbit IgG and AF647-conjugated-anti-mouse IgG for 2 h in the dark.

Table 1. Patient characteristics for the primary tumor cases

Number of patients	90
Age	
Median	70
Range	40–91
≤70	46
>70	44
Gleason score	
<7	0
7	57
>7	33
pT-status	
T2c	39
T3a	17
T3b	32
T4	2
pN-status	
N0	19
N1	38
n.d.	33
Perineural invasion	
Yes	61
No	4
n.d.	25
Angiolymphatic invasion	
Yes	33
No	44
n.d.	13

n.d., not determined.

After washing, slides were incubated with AF488-conjugated pan-CK mouse antibody (53-9003-82, Thermo Fisher, Carlsbad, CA, USA) at 1:100 and DAPI for 2-h in the dark. IHC for CD3 followed our previous method using anti-CD3 antibody (A0452, DAKO, Santa Clara, CA, USA) at 1:200 [7].

Microscopy and quantification of PMN-MDSCs

The fluorescently stained slides were imaged with Leica DMi8. For each tissue section, 2–4 images were taken with the ×20 objective and loaded to ImageJ (NIH) for counting CD11b⁺ CD15⁺ cells. The calculated densities were averaged as PMN-MDSC density for the section. We defined epithelial and stromal compartments as being immediately within or outside the outer cell layer of epithelial islands, respectively. For lymph node and bone metastases, tumor regions were defined on the basis of where pan-CK⁺ cells reached, which was assisted by locating carcinoma islands on the H&E section. Regions outside the periphery of pan-CK⁺ islands were considered to belong to the lymphoid organ. Within the neoplastic regions, epithelial and stromal areas were denoted similarly as in primary tumors. Because bone marrow contains preexisting granulocytes which may also stain positively with CD11b and CD15, we excluded those

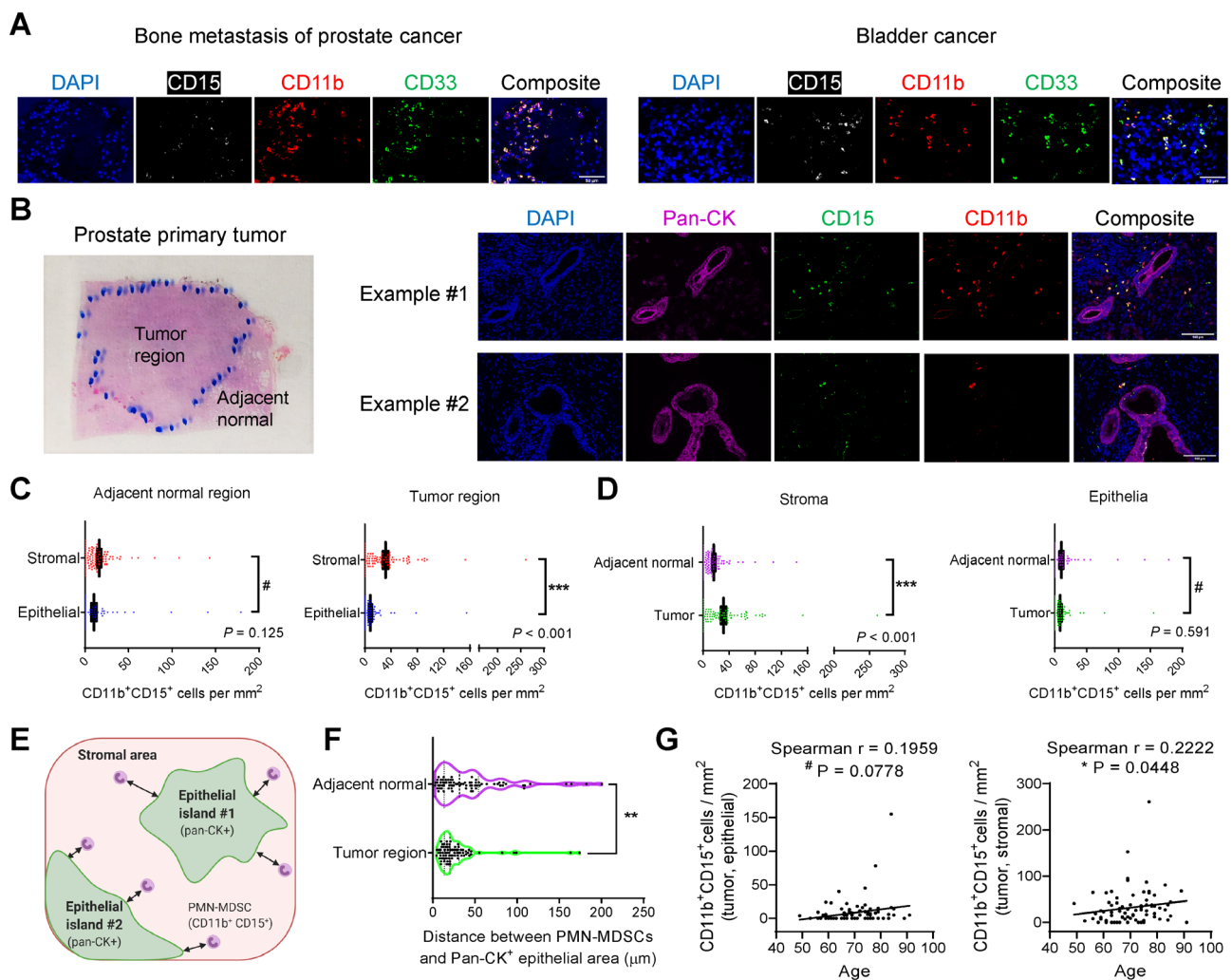


Figure 1. Increased infiltration of CD11b⁺ CD15⁺ PMN-MDSCs in the stromal areas but not epithelial areas of primary prostate tumors. (A) Representative images of bone metastasis of PCa and bladder cancer showing the overlapping staining pattern of CD11b and CD33. Scale bar, 50 μm. (B) Representative image of a prostate tumor section with contours of the tumor and adjacent normal regions drawn by the pathologist, and two representative image sets of primary prostate tumors stained with the CD11b/CD15/pan-CK/DAPI mIF panel. Scale bar, 100 μm. (C,D) Quantification results of CD11b⁺CD15⁺ PMN-MDSCs. $N = 90$. Data represent mean \pm standard error of the mean (SEM). P values calculated using a negative binomial regression model. (E) Illustration of the definition of epithelial area, stromal area and the distance between PMN-MDSCs and nearest epithelial edge. (F) Violin plot comparing the distance between PMN-MDSCs and the nearest epithelial area in the tumor and adjacent normal regions. $**p = 0.0011$ by Wilcoxon matched-pair test. (G) Association of stroma-residing PMN-MDSCs, but not epithelia-residing PMN-MDSCs, in primary tumors with patient age ($N = 90$), tested by two-tailed Spearman test.

cells by only analyzing CD11b⁺ CD15⁺ infiltrating PMN-MDSCs in the tumor regions.

Statistical analysis

For comparison between PMN-MDSC groups, we used the negative binomial regression model to calculate P values (R package). This method is appropriate to analyze the over-dispersed count outcome variables [6]. Other tests are noted in figure legends. P values less than 0.05 were considered significant.

Results

PMN-MDSCs infiltrate more abundantly in the stroma than the epithelia

PMN-MDSCs were stained as CD11b⁺ CD33⁺ CD15⁺ cells in PCa [6]. We stained CD11b, CD33, CD15 in a number of prostate and bladder cancer samples, and observed largely overlapping staining patterns for CD11b and CD33 (Figure 1A). Therefore, we simplified the detection of PMN-MDSCs as CD11b⁺ CD15⁺ cells,

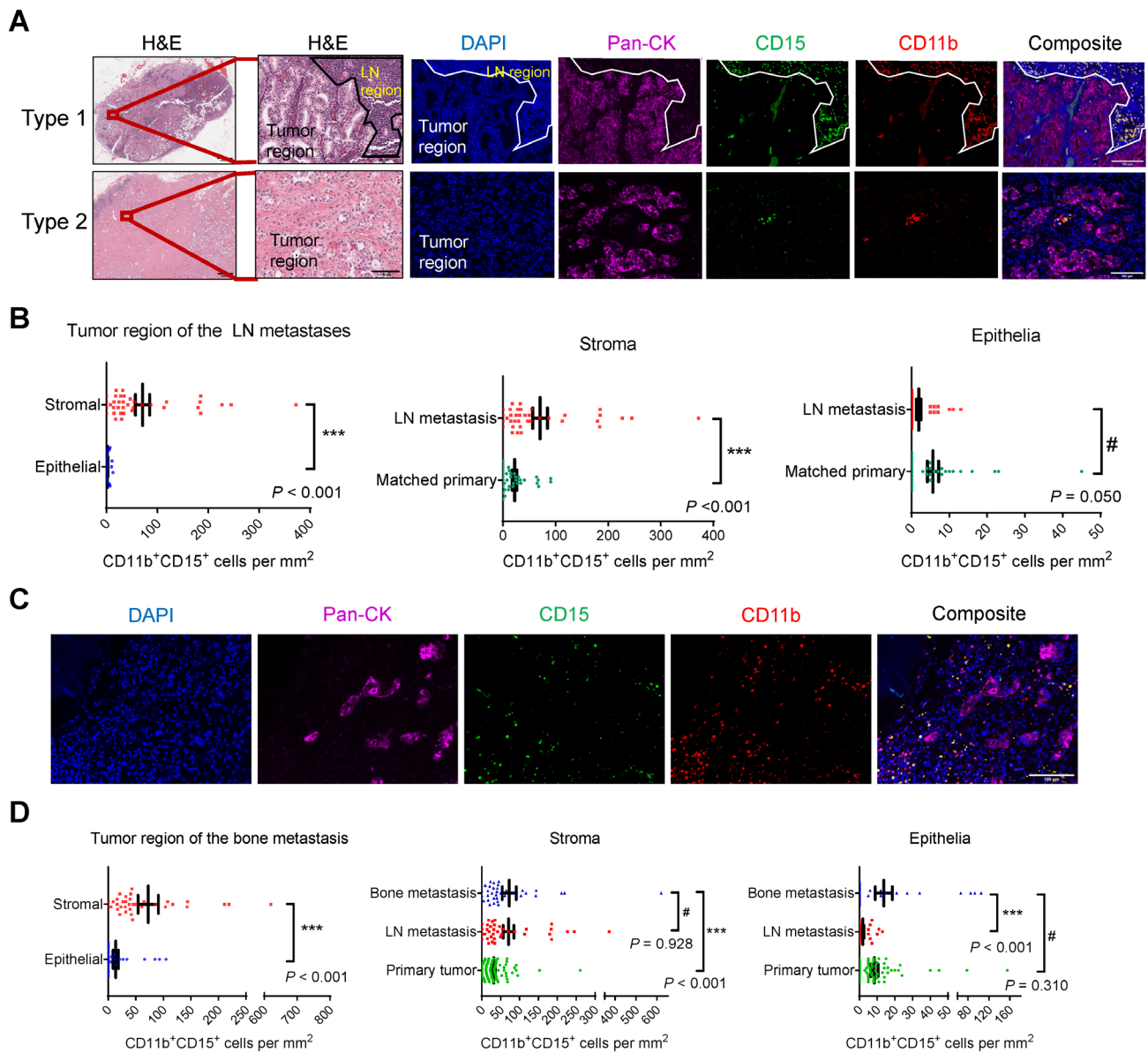


Figure 2. Higher infiltration of PMN-MDSCs in the stromal area of lymph node and bone metastases compared with the stromal area of primary tumors. (A) Representative images of the two types of lymph node metastasis samples recognized by the presence or absence of the lymph node/tumor interface in the H&E stain. Also shown are representative images of the lymph node metastasis samples stained with the CD11b/CD15/pan-CK/DAPI mIF panel. Scale bar, H&E (left), 1000 μ m; H&E (right) and IF images, 100 μ m. (B) Quantification results of CD11b⁺CD15⁺ PMN-MDSCs. $N = 37$ pairs of matched primary tumor and lymph node metastasis samples. (C) Representative images of the bone metastasis samples stained with the CD11b/CD15/pan-CK/DAPI mIF panel. Scale bar, 100 μ m. (D) Quantification results of CD11b⁺CD15⁺ PMN-MDSCs. $N = 35, 37$ and 90 for bone metastases, lymph node metastases and primary tumors, respectively. In (B) and (D), data represent mean \pm SEM. P values calculated using a negative binomial regression model.

and used pan-CK to identify epithelial cancer cells and DAPI as a nuclear stain. H&E slides of primary tumors ($N = 90$) were inspected by the pathologist (W.K.) to demarcate the tumor and adjacent normal regions (Figure 1B, left). Next, we stained the samples with the CD11b/CD15/pan-CK/DAPI mIF panel (Figure 1B,

right) and imaged both tumor and adjacent normal regions. In the adjacent normal region, PMN-MDSC infiltration was low and there was no difference between the epithelia and stroma (Figure 1C, left). By contrast, in the tumor region, the density of PMN-MDSCs was markedly higher in the stroma than the epithelia

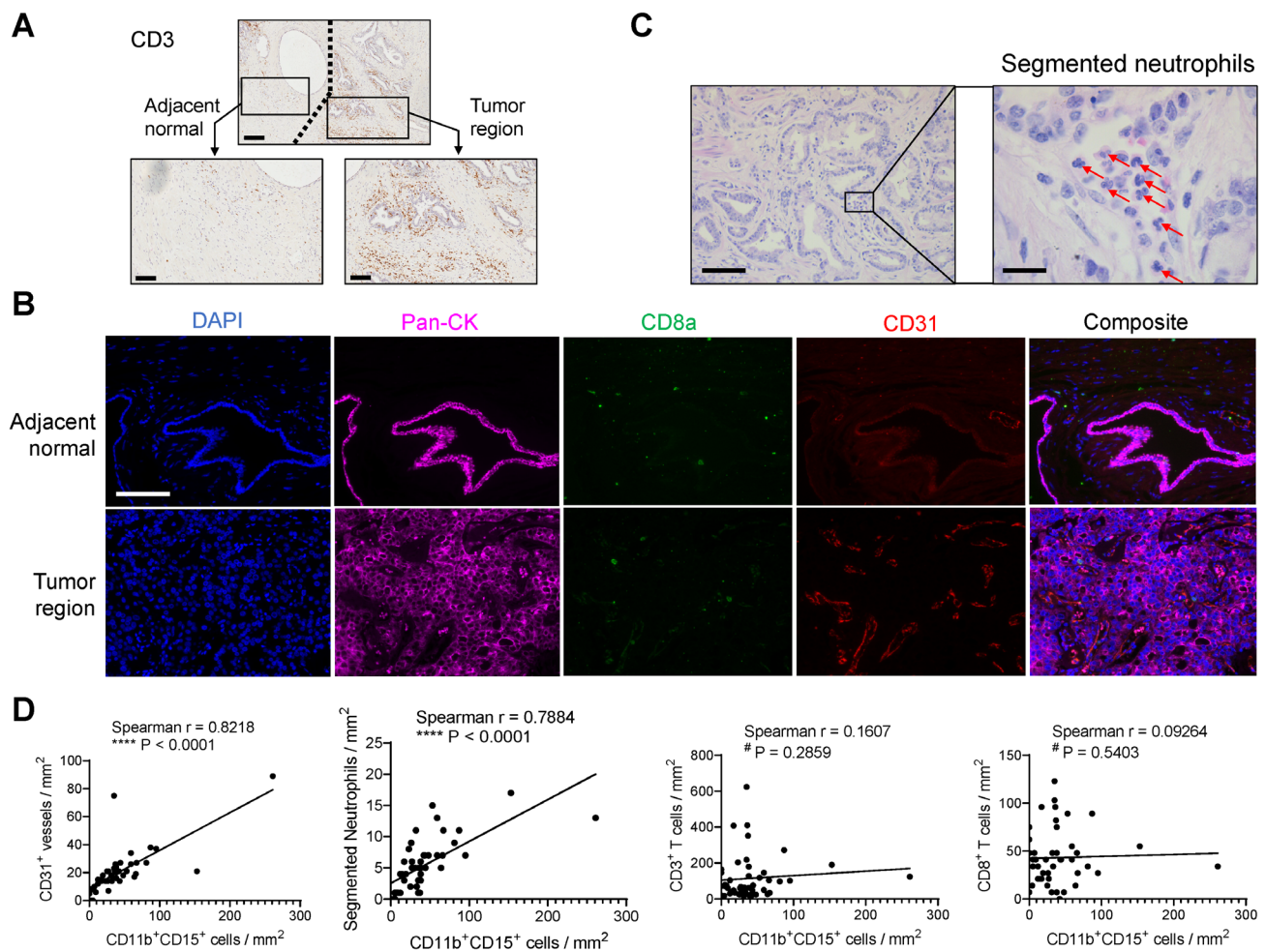


Figure 3. Positive correlation of tumor stromal PMN-MDSCs with vascularization and segmented neutrophils, evaluated using primary tumor samples ($N = 46$, SBMF). (A) Representative IHC images of CD3. Scale bar, 200 μm (top) and 100 μm (bottom). (B) Representative images of primary tumor stained with the CD31/CD8a/pan-CK/DAPI mIF panel. Scale bar, 100 μm . (C) Representative images of visually recognized segmented neutrophils (red arrows). Scale bar, 100 μm (left) and 20 μm (right). (D) Correlation analysis of the numbers of tumor stromal PMN-MDSCs with CD31⁺ vessels, segmented neutrophils, CD3⁺ total T cells, and CD8⁺ cytotoxic T cells, tested by two-tailed Spearman test.

(Figure 1C, right). When epithelia or stroma were compared between tumor and adjacent normal regions respectively, higher PMN-MDSC infiltration in tumor regions was observed for the stroma (Figure 1D, left) but not the epithelia (Figure 1D, right). These results indicate that the majority of the increased PMN-MDSC infiltration in primary prostate tumors occurs in the stroma instead of the epithelia.

We hypothesize that, in comparison with adjacent normal epithelia, neoplastic epithelia have stronger ability to attract PMN-MDSCs. To test this hypothesis, we used ImageJ (NIH, Bethesda, MD, USA) to measure the distance of all detected PMN-MDSCs to the nearest edge of the pan-CK⁺ epithelial islands on the captured

images (Figure 1E), a method applied to both the tumor and the adjacent normal regions. Confirming our hypothesis, the average distance of nearest stromal PMN-MDSCs to adjacent epithelial areas was indeed significantly shorter for the tumor region than the adjacent normal region (Figure 1F). We examined the association of stroma- or epithelia-residing PMN-MDSCs with available clinicopathological parameters (Table 1). There was no correlation of either PMN-MDSC population with Gleason score, primary tumor stage, lymph node metastasis, angiolymphatic invasion, or perineural invasion (data not shown). However, there was a significant association of stroma-residing (but not epithelia-residing) PMN-MDSCs with age (Figure 1G).

Higher PMN-MDSC infiltration in the stroma of lymph node and bone metastases than the stroma of the primary tumors

With 37 matched pairs of lymph node metastasis and primary tumor samples, we first performed H&E staining of the lymph node metastasis samples and noted two types of tumor histology. In Type 1, lymph node tissue (i.e. immune cells) shared interface with metastases; in Type 2, the whole sample was occupied by metastases (Figure 2A). We stained the samples with the mIF panel and focused our analysis on the neoplastic regions so the lymph node immune cells did not interfere (Figure 2A). Similar to the primary tumors, PMN-MDSCs were mainly found in the stroma and only sporadically seen in the epithelia (Figure 2B, left). Moreover, there was a higher PMN-MDSC infiltration in the metastasis stroma than the primary tumor stroma (Figure 2B, center). For the epithelia, there was a trend of lower PMN-MDSC density in metastases than primary tumors (Figure 2B, right).

Next, we stained 35 cases of bone metastasis (Figure 2C) and focused on the neoplastic region for image analysis. There were again significantly higher PMN-MDSCs in the stroma than the epithelia (Figure 2D, left). Next, we compared bone metastases with lymph node metastasis and all primary tumors by separating them into the stromal and epithelial areas. For the stroma, bone metastases showed a level of PMN-MDSC infiltration comparable with lymph node metastases but significantly higher than primary tumors (Figure 2D, center). For the epithelia, bone metastases displayed a PMN-MDSC density comparable with primary tumors but significantly higher than lymph node metastases (Figure 2D, right). Overall, the stroma of both bone and lymph node metastases contained higher PMN-MDSCs than that of primary tumors.

Positive correlation of tumor stromal PMN-MDSCs with vascularization and segmented neutrophils

To examine the correlation of PMN-MDSCs with vascularization and other tumor-infiltrating immune cells, we focused on 46 primary tumors from SBMF that had more specimens and performed IHC staining for CD3 (Figure 3A) and mIF staining of a CD8a/CD31/pan-CK/DAPI panel (Figure 3B). Moreover, we counted classical neutrophils based on segmented nuclear morphology using H&E slides (Figure 3C). Given that the majority of PMN-MDSCs are enriched in the tumor stroma, we focused on this compartment and found that PMN-MDSCs significantly correlated with CD31+

vessels and segmented neutrophils, but not CD3+ or CD8+ T cells (Figure 3D).

Discussion

Our studies reveal that (1) in all three sites, PMN-MDSCs infiltrate much more readily in the stroma than the epithelia; (2) metastasis stroma is infiltrated with more PMN-MDSCs than that of primary tumors; (3) prostate epithelia remain weakly infiltrated by PMN-MDSCs even when transformed. This result suggests that paracrine signaling between PMN-MDSCs and PCa cells through IL-1Ra and IL-23 [6,8] should require efficient cytokine diffusion. The stromal enrichment of PMN-MDSCs facilitates cell-cell contact between PMN-MDSCs and T cells to mediate the suppression [9,10], a result in line with the current view of the greater relevance of PMN-MDSCs in the stroma [11]. One limitation of our study is the lack of healthy prostate tissues as control. Previous studies have shown a very low frequency (<1%) of circulating CD15^{high} CD33^{low} cells in healthy donors [5], consistent with the notion that MDSCs are typically absent at steady state in healthy individuals [2].

At least two mechanisms may explain why metastases are infiltrated with more PMN-MDSCs than primary tumors. First, PMN-MDSCs expand dramatically in lymphoid organs [12,13]. Therefore, colonized tumors in the bone marrow or lymph nodes are expected to be more readily accessible to nearby PMN-MDSCs compared with the situation of the primary tumor where PMN-MDSCs need to travel distantly before reaching the tumor parenchyma. Second, metastatic PCa cells may produce higher levels of MDSC-recruiting chemokines than primary tumor cells. CXCL5/CXCR2 signaling plays a crucial role in PMN-MDSC recruitment in PCa [14]. CXCL5 expression is concordant with PCa progression with the highest level in metastases [15]. Therefore, it is possible that higher CXCL5 in metastases drives stronger PMN-MDSC infiltration. Bone is the most frequent site of PCa metastasis [16]. For metastases to nonlymphoid organs such as lung and liver, future research should examine whether they also harbor higher PMN-MDSCs than primary tumors.

The lack of correlation of PMN-MDSCs with T cells suggests that other immunosuppressive cells (such as T_{reg} and M2 macrophages) should also contribute to the immunologically cold microenvironment of PCa. The association of tumor stromal PMN-MDSCs with age is interesting, because circulating PMN-MDSCs (but not M-MDSCs) are significantly

elevated during aging [17]. Since age is the biggest risk factor for PCa, it will be important to determine whether higher PMN-MDSCs in older men is a driver for increased PCa rate.

Acknowledgements

We thank Dr. Qing Li and the pathology department at SBMF. We thank Dr. Patricia Troncoso and the pathology department at MDACC. This research was partly supported by the institutional fund from University of Notre Dame. J. Wen, GH, and X. Wen were partly supported by National Natural Science Foundation of China General Program (Grant No. 817773047). X. Wang and CZ were supported by the Featured Clinical Discipline Project of Shanghai Pudong (Grant No. PWZzb2017-06) and National Key Research and Development Program of China (Grant No. 2017YFA 0103902). J. Wan was supported by the IU Simon Cancer Center (Grant P30CA082709), the Purdue University Center for Cancer Research (Grant P30CA023168), Walther Cancer Foundation, and Indiana University Precision Health Initiative (PHI).

Author contributions statement

X. Wen and XL designed the study. J. Wen, GH, and YZ acquired the data. J. Wen, GH, SL, J. Wan, X. Wang, and WK analyzed the data. LC contributed to the clinical resource. CZ, X. Wen, and XL supervised the project. J. Wen, GH, and XL wrote the manuscript.

References

1. Veglia F, Perego M, Gabrilovich D. Myeloid-derived suppressor cells coming of age. *Nat Immunol* 2018; **19**: 108–119.
2. Gabrilovich DI. Myeloid-derived suppressor cells. *Cancer Immunol Res* 2017; **5**: 3–8.
3. Torre LA, Bray F, Siegel RL, *et al.* Global cancer statistics, 2012. *CA Cancer J Clin* 2015; **65**: 87–108.
4. Lu X, Horner JW, Paul E, *et al.* Effective combinatorial immunotherapy for castration-resistant prostate cancer. *Nature* 2017; **543**: 728–732.
5. Hossain DM, Pal SK, Moreira D, *et al.* TLR9-targeted STAT3 silencing abrogates immunosuppressive activity of myeloid-derived suppressor cells from prostate cancer patients. *Clin Cancer Res* 2015; **21**: 3771–3782.
6. Calcinotto A, Spataro C, Zagato E, *et al.* IL-23 secreted by myeloid cells drives castration-resistant prostate cancer. *Nature* 2018; **559**: 363–369.
7. Feng S, Cheng X, Zhang L, *et al.* Myeloid-derived suppressor cells inhibit T cell activation through nitrating LCK in mouse cancers. *Proc Natl Acad Sci U S A* 2018; **115**: 10094–10099.
8. Di Mitri D, Toso A, Chen JJ, *et al.* Tumour-infiltrating Gr-1+ myeloid cells antagonize senescence in cancer. *Nature* 2014; **515**: 134–137.
9. Yuan H, Hsiao YH, Zhang Y, *et al.* Destructive impact of T-lymphocytes, NK and mast cells on basal cell layers: implications for tumor invasion. *BMC Cancer* 2013; **13**: 258.
10. Flammiger A, Bayer F, Cirugeda-Kühnert A, *et al.* Intratumoral T but not B lymphocytes are related to clinical outcome in prostate cancer. *APMIS* 2012; **120**: 901–908.
11. Zhou J, Nefedova Y, Lei A, *et al.* Neutrophils and PMN-MDSC: their biological role and interaction with stromal cells. *Semin Immunol* 2018; **35**: 19–28.
12. Youn JI, Nagaraj S, Collazo M, *et al.* Subsets of myeloid-derived suppressor cells in tumor-bearing mice. *J Immunol* 2008; **181**: 5791–5802.
13. Nagaraj S, Youn JI, Gabrilovich DI. Reciprocal relationship between myeloid-derived suppressor cells and T cells. *J Immunol* 2013; **191**: 17–23.
14. Wang G, Lu X, Dey P, *et al.* Targeting YAP-dependent MDSC infiltration impairs tumor progression. *Cancer Discov* 2016; **6**: 80–95.
15. Begley LA, Kasina S, Mehra R, *et al.* CXCL5 promotes prostate cancer progression. *Neoplasia* 2008; **10**: 244–254.
16. Gartrell BA, Saad F. Managing bone metastases and reducing skeletal related events in prostate cancer. *Nat Rev Clin Oncol* 2014; **11**: 335–345.
17. Alves AS, Ishimura ME, Duarte YAO, *et al.* Parameters of the immune system and vitamin D levels in old individuals. *Front Immunol* 2018; **9**: 1122.